Journal of Advanced Research 67 (2025) 373–386

Contents lists available at ScienceDirect

Journal of Advanced Research

journal homepage: www.elsevier.com/locate/jare

Veterinary Medicine

Chronic arsenic exposure-provoked biotoxicity involved in liver-microbiota-gut axis disruption in chickens based on multi-omics technologies

Jiayi Li [a], Changming Guo [b], Yan Liu [a], Biqi Han [a], Zhanjun Lv [a], Huijie Jiang [a], Siyu Li [a], Zhigang Zhang [a,*]

[a] College of Veterinary Medicine, Northeast Agricultural University, 600 Changjiang Road, Harbin 150030, China
[b] College of Veterinary Medicine, Jilin University, Changchun, China

HIGHLIGHTS

- Transcriptomic, metabolome, and 16S rRNA sequencing reveal chronic arsenic toxicity.
- Arsenic treatment induced chicken liver dysfunction and ileum microbiota dysbiosis.
- Chronic inorganic arsenic exposure evidently promoted liver fibrosis in chickens.
- Long-term arsenic exposure disrupted enterohepatic circulation of bile acid.
- Arsenic exposure provoked liver-microbiota-gut axis disruption in chickens.

GRAPHICAL ABSTRACT

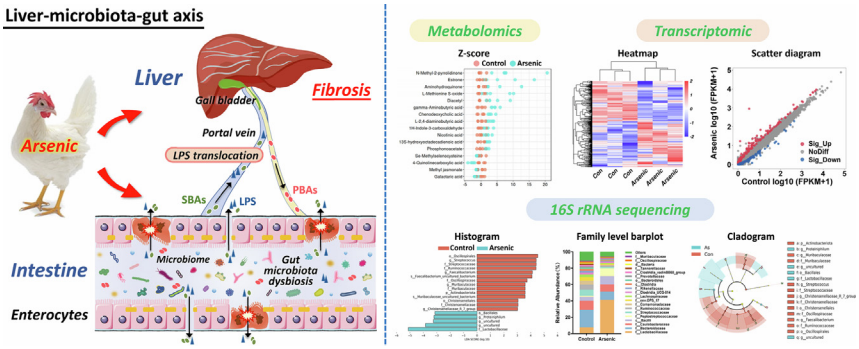

ARTICLE INFO

Article history:
Received 19 December 2022
Revised 27 October 2023
Accepted 13 January 2024
Available online 17 January 2024

Keywords:
Chronic arsenic exposure
Liver-microbiota-gut axis
Liver fibrosis
Ileal microbiota
Bile acids
Multi-omics technologies

ABSTRACT

Introduction: Arsenic has been ranked as the most hazardous substance by the U.S. Agency for Toxic Substances and Disease Registry. Environmental arsenic exposure-evoked health risks have become a vital public health concern worldwide owing to the widespread existence of arsenic. Multi-omics is a revolutionary technique to data analysis providing an integrated view of bioinformation for comprehensively and systematically understanding the elaborate mechanism of diseases.
Objectives: This study aimed at uncovering the potential contribution of liver-microbiota-gut axis in chronic inorganic arsenic exposure-triggered biotoxicity in chickens based on multi-omics technologies.
Methods: Forty Hy-Line W-80 laying hens were chronically exposed to sodium arsenite with a dose-dependent manner (administered with drinking water containing 10, 20, or 30 mg/L arsenic, respectively) for 42 d, followed by transcriptomics, serum non-targeted metabolome, and 16S ribosomal RNA gene sequencing accordingly.
Results: Arsenic intervention induced a serious of chicken liver dysfunction, especially severe liver fibrosis, simultaneously altered ileal microbiota populations, impaired chicken intestinal barrier, further drove enterogenous lipopolysaccharides translocation via portal vein circulation aggravating liver damage. Furtherly, the injured liver disturbed bile acids (BAs) homoeostasis through strongly up-regulating the BAs synthesis key rate-limiting enzyme CYP7A1, inducing excessive serum total BAs accumulation, accompanied by the massive synthesis of primary BA—chenodeoxycholic acid. Moreover, the concentrations of secondary BAs—ursodeoxycholic acid and lithocholic acid were markedly repressed, which might involve in the repressed dehydroxylation of *Ruminococcaceae* and *Lachnospiraceae* families. Abnormal BAs metabolism in turn promoted intestinal injury, ultimately perpetuating pernicious circle in chickens.

* Corresponding author at: College of Veterinary Medicine, Northeast Agricultural University, No. 600 Changjiang Road, Harbin 150030, China.
E-mail address: zhangzhigang@neau.edu.cn (Z. Zhang).

https://doi.org/10.1016/j.jare.2024.01.019

Notably, obvious depletion in the abundance of four profitable microbiota, *Christensenellaceae*, *Ruminococcaceae*, *Muribaculaceae*, and *Faecalibacterium*, were correlated tightly with this hepato-intestinal circulation process in chickens exposed to arsenic.

Conclusion: Our study demonstrates that chronic inorganic arsenic exposure evokes liver-microbiota-gut axis disruption in chickens and establishes a scientific basis for evaluating health risk induced by environmental pollutant arsenic.

Introduction

In 2007, the U.S. Agency for Toxic Substances and Disease Registry has ranked arsenic at the top of the Substance Priority List, declaring the highest terrific toxicity of environmental arsenic exposure for human and animal health [1]. As a ubiquitous metalloid element, arsenic has been inevitably released into soil, groundwater, and atmosphere owing to natural and human activities [2,3]. Up to the present, groundwater arsenic contamination is still posing a major public health threat [4]. Consuming arsenic-polluted water is the predominant route for environmental arsenic to invade human body, directly leading to arsenic poisoning [5,6]. In 2001, the United States Environmental Protection Agency (US EPA) has instituted the maximum arsenic recommended limit of 10 part per billion in drinking water [7]. About 94 to 220 million people have been potentially persecuted by high concentrations of arsenic in groundwater, involving a large number of countries [2,8].

Liver is a vital detoxifying and metabolic organ, which is vulnerable to exogenous toxins [9,10]. Hepatotoxicity is persuasively considered as the key to risk assessment and possesses common toxic characteristic of various environmental contaminants. Recently, accumulated evidences consequently focus on arsenic exposure-induced hepatotoxicity. Liver fibrosis is an adverse outcome of chronic and repeated liver damage, leading to excessive extracellular matrixes (ECM) deposition including collagens and fibronectin on the basis of the imbalance between fibrogenesis and fibrolysis [11]. While without timely intervention, liver fibrosis may irreversibly develop into liver cirrhosis, which collectively caused the deaths of approximately 1.3 million people worldwide per year [12]. Moreover, the activation and *trans*-differentiation of hepatic stellate cells (HSCs) into myofibroblasts functionally involve in the central events of liver fibrosis [13]. In recent years, toxicological evidences have demonstrated that arsenic can induce HSCs activation and liver fibrosis [14]. Generally, chickens (*Gallus gallus*) occupy an unshakable position in the poultry industry with large breeding scale and quantity, constituting the major source of animal protein [15]. Up to now, whether chronic inorganic arsenic exposure may contribute to liver fibrosis in chickens remain need to be interrogated urgently, which is helpful for human to fully understand the mechanism of arsenic-induced hepatotoxicity.

The liver-gut axis refers to the intricate bidirectional interaction between liver and gut microbiota integrated by the signals of genetic, dietary, and environmental factors [16]. Functionally, the systemic circulation, portal vein, and biliary tract are responsible for the maintenance of their reciprocal communication [17]. To be specific, gut-derived products directly migrate to the liver via the portal vein, likewise, the liver secrets the bile and antibody to the intestine in a feedback manner, which collectively establishing the reciprocal action between the liver and the microbiome [16]. It should be noted that bile acids (BAs) synthesized from cholesterol (CHO) in the liver, involves in a host of metabolic regulation as endogenous ligands via the interaction with nuclear receptors [18]. Importantly, the variety of BAs has been proven to be largely determined by the gut microbiome [19]. Hence, the possible role of BAs in tightly linking liver-microbiota-gut axis remains deserving to be explored in depth. It is interesting to elucidate the toxicological effect of arsenic on liver-microbiota-gut axis for evaluating the harmful risks of arsenic exposure.

Multi-omics is a revolutionary technique to data analysis providing a comprehensive view of biological information simultaneously integrated from multiple levels, enables researchers to comprehensively understand the elaborate mechanism of diseases for better investigating targeted treatment. In this study, we have conducted the integrated analyses of transcriptomics, serum non-targeted metabolome, and 16S ribosomal RNA (rRNA) gene sequencing, and aimed to uncover the potential contribution of liver-microbiota-gut axis in arsenic exposure-induced biotoxicity. To our knowledge, this is the first study using the multi-omics technologies to comprehensively and systematically investigate harmful effect and mechanism of arsenic exposure in chickens.

Materials and methods

Animal models

Hy-Line W-80 laying hens (19 d of age, weighting 120 ± 20 g, female) from the Experimental Animal Centre of Harbin Veterinary Research Institute of Chinese Academy of Agricultural Sciences (Harbin, China) were domesticated in facilities (22 ± 2 °C, 55 ± 5 %). A total of 40 chickens were distributed into 4 groups (n = 10) randomly provided standard chow *ad libitum* under a light–dark (12:12) cycle. After the chickens were acclimated for one-week, the formal experiment was carried out.

Experimental design

Sodium arsenite (purity ≥ 90 %) was from Sigma-Aldrich (United States). Different doses of sodium arsenite were dissolved with conventional drinking water. Four-group chickens were administered with drinking water containing 0 mg/L, 17.3 mg/L, 34.7 mg/L, or 52 mg/L sodium arsenite (corresponding to 0, 10, 20, or 30 mg/L arsenic, respectively), and the design of the trial dose gradient was based on previous studies and our pre-trial [5,20,21]. The test duration was 42 d. At the last administration, the chickens were fasted and sacrificed, then the blood from wing root vein was harvested for serum samples detection. Parts of liver tissues, serum samples, and ileum content were collected and sent to E-GENE Technology Co., Ltd (Shenzhen, China) for multi-omics sequencing.

Ethics statement

All experiments involving animals were conducted according to the ethical policies and procedures approved by the Animal Ethics Committee of Northeast Agricultural University (Approval no. 202104118).

Biochemical indicators and redox status evaluation

After the blood were centrifuged, the serum samples were collected for biochemical indexes detection. The levels of conventional biochemical indexes including aspartate aminotransferase (AST), alanine aminotransferase (ALT), alkaline phosphatase (ALP), total cholesterol (TCHO), triglyceride (TG), low density lipoprotein (LDL), high density lipoprotein (HDL), and total bile acid (TBA) in serum were assessed using a Beckman Coulter DxC800 biochemical analyzer (CA, USA) or Toshiba TBA-2000FR automatic biochemical analyzer (Tokyo, Japan).

Liver tissues were partly homogenized using a high-throughput tissue grinder (Scientz-48L, Ningbo Scientz Biotechnology Co., Ltd, Ningbo, China), then centrifuged for assessing the glutathione (GSH) concentration, superoxide dismutase (SOD) activity, and malondialdehyde (MDA) content strictly following the manufacturer's instruction (Jiancheng Bioengineering Institute, Nanjing, China) [22].

Histopathological analysis

Histopathological analysis was performed to visually observe the tissue injury and evaluate the extent of lesion. Liver tissues and ileum samples were cut, fixed in 4 % paraformaldehyde, dehydrated, and embedded with paraffin. Subsequently, dewaxed slices were conducted for haematoxylin and eosin (H&E), Sirius red, and Masson's trichrome staining. The morphology was randomly captured with microscope (Olympus BX-FM, Tokyo, Japan) or a polarized light microscope (Olympus, Japan), respectively.

The transmission electron microscopy (TEM) observation protocol was roughly executed as follows. The trimmed liver tissues were immersed with 2.5 % glutaric dialdehyde and fixed with 1 % osmium tetroxide [23]. The fixed slices were rinsed and dehydrated with gradient elution and acetone. Finally, the samples were cut for staining with uranyl acetate and lead citrate and the observation with TEM (TEM, Hitachi H-7650, Tokyo, Japan).

Oil red O staining was used for detecting the lipid content in liver [24]. Simply, frozen slices were cut and stained with Oil Red O working solution, then redyed with hematoxylin. Finally, the light microscopy was used for examining the stained sections (Olympus BX-FM, Tokyo, Japan).

Terminal deoxynucleotidyl staining assay

Terminal deoxynucleotidyl transferase dUTP nick-end labeling (TUNEL) kit was applied to assay apoptosis based on labeling the free 3′-hydroxyl termini of genomic DNA breakage. The operation was completely according to the producer's protocol [25].

Hydroxyproline and lipopolysaccharides assay

Alkaline hydrolysis colorimetry was conducted to measure liver hydroxyproline (HYP) content for evaluating the severity of fibrosis. Concretely, liver tissues were fully hydrolyzed for 20 min, then pH value of the total liquid was adjusted. Accordingly, the tissues were bathed in water and centrifuged. Finally, the supernatant was collected for reading absorbance (550 nm) with a microplate reader (SpectraMax Absorbance Reader Cmax Plus, Shanghai, China) [26].

The Chicken Lipopolysaccharide (LPS) Elisa Assay Kit (REF. H255-1–1) specifically customized from Nanjing Jiancheng Bioengineering Institute (Nanjing, China) was applied for detecting the level of chicken serum LPS by competition method. Specifically, the samples were added to enzyme well (pre-coated with antibodies), then mixed with recognition antigen labeled by horse radish peroxidase (HRP), incubating for 1 h at 37 °C. The samples and recognition antigen both competed for solid phase antigen and formed immune complex. After washed with phosphate buffered solution, the combined HRP catalyzed Tetramethyl benzidine into blue, and turned into yellow by the action of acid. Finally, the optical density was measured under 450 nm wavelength with a microplate reader (SpectraMax Absorbance Reader Cmax Plus, Shanghai, China). The LPS levels of serum were calculated according to the concentration and optical density values.

Hepatic transcriptome sequencing and enrichment analysis

Liver total RNA was collected and prepared from frozen tissues for transcriptome sequencing. RNA quantification and qualification (purity, integrity, and concentration) was carried out in advance. Equal volume of RNA was input for preparations. The NEBNext® UltraTM RNA Library Prep Kit for Illumina® (NEB, USA) was used for generating sequencing libraries. An adjusted p-value ≤ 0.05 and absolute fold-change ≥ 2 were set for differential expression genes (DEGs) filtration [27]. Moreover, Metascape database (https://metascape.org/), a robust online database, integrated enrichment genes' potential biological functions and process enrichment analysis [28].

16S ribosomal RNA gene sequencing

For the identification and taxonomic classification of bacterial species, 16S rRNA gene sequencing analysis was involved in the present study. Chicken ileal content were sampled. Total microbial DNA was extracted with a QIAamp DNA stool extraction kit (Qiagen, Germany). The genomic DNA was analyzed by agarose gel electrophoresis and quantified by Qubit 2.0 Fluorometer (ThermoFisher Scientific, USA). Subsequently, the bacterial V3-V4 hypervariable region of the 16S rRNA gene was amplified with PCR and the amplicons was purified using AMPure XP Beads (Beckman Coulter, USA). Subsequently, the sequencing libraries were generated and library quality was assessed. The quality libraries were finally sequenced on an Illumina HiSeq 2500 platform according to the manufacturer's guidelines.

Serum non-targeted metabolomic analysis

After the sample preparation, 200 μL serum per sample was obtained and adequately mixed with methanol (400 μL) for supernatant collection. Then the samples were concentrated to dry in vacuum, and re-dissolved with 2-chlorobenzalanine 80 % methanol solution. Liquid chromatography mass spectrometry (LC-MS) was performed for detecting filtered-supernatant samples.

Chromatographic separation was accomplished by an Ultimate 3000 system equipped with an ACQUITY UPLC® HSS T3 (Thermo, USA). The analytes were gradient-eluted and samples were injected after equilibration. After setting up the parameters, scanning of the Orbitrap analyzer and data dependent acquisition MS/MS experiments were conducted [29].

Quantitative real-time PCR assay and western blot assay

Isolated total RNA was reverse-transcribed into cDNA following the manufacturer [30,31]. The quantitative real-time PCR (qRT-PCR) was performed with a Bio-Rad CFX96 touch (Hercules, CA, USA) based on 2 × AceQ Universal SYBR Green RT-qPCR SuperMix (Vazyme Biotech Co., ltd) with primers sequences (shown in Table S1) [32]. The standard method ($2^{-\Delta\Delta Ct}$) was used for calculating relative RNA levels of samples [33].

For the immunodetection and analysis of specific proteins, liver samples were lysed by homogenization for extracting proteins. The BCA protein quantification kit (Beyotime, Jiangsu, China) was used

to measure protein concentrations [34,35]. After separated by SDS-PAGE, the proteins were transferred from the gel to polyvinylidene difluoride membranes [36]. Then the membranes were successively incubated with primary antibodies and horseradish peroxidaseconjugated secondary antibodies [37]. Primary antibodies against alpha-smooth muscle actin (α-SMA), Smad2, tumor necrosis factor alpha (TNF-α), nuclear factor-kappa B (NF-κB), and Lamin B were from Bioss Biotechnology (Beijing, China). Occludin (OCLN) antibody (Proteintech, Wuhan, China), Claudin-1 (CLDN1) antibody (Catalog No. A2196, Abclonal, Wuhan, China), and Sirtuins 6 (Sirt6) antibody (Beyotime, Shanghai, China) were purchased. The antibody to glyceraldehyde-3-phosphate dehydrogenase (GAPDH) was from Hangzhou Goodhere Biotechnology (Hangzhou, China). Secondary antibodies were from ZSGB-BIO (Beijing, China). The blots were enhanced and visualized by chemiluminescence light. Image Pro-Plus 6.0 software (Rockville, MD, USA) was eventually used for determining quantitative bands intensity [38].

Protein-protein interaction analysis

Protein-protein interaction (PPI) detection was constructed for predicting present study-related multiple proteins and the visualizing based on the integrated data requesting from STRING database (https://string-db.org/, Version 11.5) [39]. Specifically, PPI network of selected species (*Gallus gallus*) was constructed for the functional interaction of the target protein.

Statistical analysis

Results were quantitatively presented as mean ± standard error (SEM). One-way analysis of variance followed by Tukey's *post hoc* test was used for groups' comparisons manipulating SPSS 23.0 (SPSS, Chicago). A value of $p < 0.05$ was considered significant. Clustering correlation heatmap were performed using the OmicStudio tools (https://www.omicstudio.cn) and ChiPlot (https://www.chiplot.online/).

Results

Arsenic administration induced liver histopathological abnormality and hepatic dysfunction in chickens

Macroscopic morphology of liver was conducted for intuitively examining tissue injury of chickens. In comparison with the control livers, arsenic-exposed livers turned pale, yellow, and fatty with a dose-dependent manner (Fig. 1A). Histopathological assessments of liver tissue structures in chickens from each group were subsequently determined.

H&E staining indicated normal hepatic structure in control chickens characterized by regular radial hepatic cords (Fig. 1B and C). Whereas, 10 mg/L arsenic-treated liver sections showed a mild disordered hepatic cord with slight central venous congestion (Fig. 1C). Similar but severer pathological changes with increased cell gap were displayed in 20 mg/L arsenic group (Fig. 1C). What's worst, livers from highest arsenic-administrated group were largely damage, along with hepatic architectural destruction, swollen hepatocytes, and extensive inflammation infiltration (Fig. 1C).

TEM was used to visualize hepatocyte ultrastructure, especially the high-resolution micrographs of mitochondria. As displayed in Fig. 1D, the control chickens presented normal hepatocyte structure with regular mitochondria morphology, cristae membranes, and cristae junctions (Fig. 1D). While arsenic-treated groups showed varying degrees of damage (Fig. 1D). In 10 mg/L arsenic group, morphology showed several swollen mitochondria, with fragmented and partially disappeared mitochondrial cristae of individual cells. Except for a similar but more variation extent to the changes we found in 10 mg/L arsenic group, 20 mg/L arsenic treatment collectively induced unclear edge of nuclear membrane and loss of mitochondrial structure (Fig. 1D). Moreover, the highest dose arsenic group showed the most severe change including fragmented and severely fuzzy mitochondrial crista, along with mitochondrial vacuolization (Fig. 1D).

Several key hepatic function-related serum biochemical indicators were detected to assess liver damage. AST, ALT, and ALP activities collectively reflected the liver function (Fig. 1E, F, and H). Likewise, the ratio of AST to ALT (AST/ALT), regarded as a clue to liver disease, was decreased dose-dependently (Fig. 1G). As shown in Fig. 1E and F, the AST and ALT activities were obviously elevated under the administration of arsenic (Fig. 1E and F). And the AST/ALT ratio showed a downward trend in the 30 mg/L arsenic group (Fig. 1G).

Arsenic administration induced liver transcriptomic alteration in chickens

Transcriptional profiling of host gene expression in chicken livers was performed for identifying the key genes participated in arsenic-induced hepatotoxicity. The similarity and heterogeneity of samples from each group were shown as a heatmap (Fig. 1I). Sequencing analysis result indicated that a total of 363 DEGs were comprising, screening out 195 upregulated genes and 168 downregulated genes, visualized as volcanic plot (Fig. 1J) and scatter diagram (Fig. 1K).

Moreover, GO functional analysis of the candidate DEGs was derived from the Metascape database (https://metascape.org/). Networks of GO enriched terms (top 20) colored by clusters (Fig. S1A) and enriched pathway interaction network of DEGs (Fig. 1L) indicated that DEGs mainly enriched in biological processes associated with metabolism of lipids, response to hormone, PPAR signaling pathway, regulation of small molecule metabolic process, cellular response to chemical stress, lipid localization, nuclear receptors *meta*-pathway, fatty acid metabolic process, mitochondrion organization, negative regulation of small molecule metabolic process, circulatory system process, response to toxic substance, multicellular organismal homeostasis, non-alcoholic fatty liver disease, response to oxidative stress, vasculature development, positive regulation of cold-induced thermogenesis, gonad development, IL-18 signaling pathway, and PID IL27 pathway (Fig. S1A and 1L). Subsequently, we classified the DEGs by functional categories, which would be elucidated in detail in corresponding sections.

Arsenic administration drove the development of liver fibrosis in chickens

Different degrees of fibrotic lesion were observed in arsenic-intervened livers of chickens, preliminarily evidenced by reliable connective tissue stain. Specifically, Masson's trichrome staining and Sirius red staining were conducted for the visual quantification of collagen fibers. Dramatical collagen fibers accumulation (blue collagen deposition in the hepatic sinusoids and central vein) in Masson's trichrome staining was presented under arsenic administration (Fig. 2A). As shown in Fig. 2B, under the ordinary light microscope, according to the scope of red-stained collagen in dewaxed sections, the fibrosis extent of the liver treated with arsenic was higher than the control liver (Fig. 2B). Further viewed under a polarized light, primary collagen I (red and yellow staining) and few collagen III (green staining) depositions were differentiated and visualized with an obviously dose-dependent manner (Fig. 2C and D). HYP levels in the liver exposed to arsenic were much higher than that in control chickens, and a markedly increase

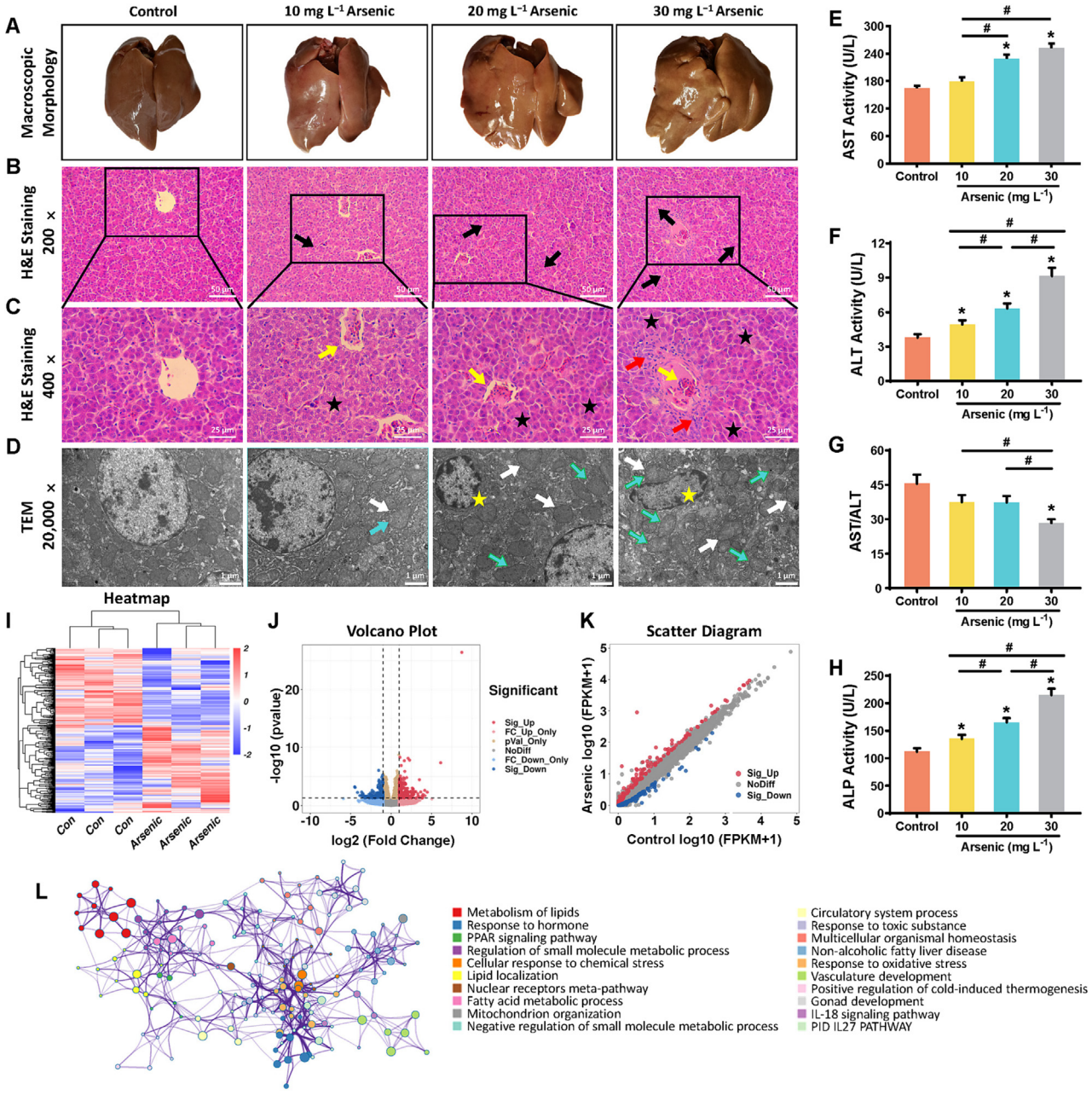

Fig. 1. Arsenic administration affected liver histology and influenced transcriptome profiling of liver in chickens. Typical macroscopic morphology (A), representative H&E staining images (B and C), and ultrastructure (D) in liver of chickens treated with/without arsenic. Black arrows: disordered hepatic cord; yellow arrows: central venous congestion; red arrows: inflammatory cell infiltration; black stars: increased cell gap (H&E staining, B: Scale bar = 50 μm, magnification 200 ×; C: Scale bar = 25 μm, magnification 400 ×). White arrows: swollen mitochondria; blue arrows: damage mitochondrial cristae structure; yellow stars: unclear edge of nuclear membranes (D: Scale bar = 1 μm, magnification 20,000 ×). AST (E), ALT (F), ALP (H) and the ratio of AST/ALT (G) from control and arsenic administration group (n = 7). Heatmaps (I), volcanic plot (J), and scatter diagram (K) of DEGs in transcriptome from the liver of control group vs. 30 mg/L arsenic group. Enriched pathway interaction network of DEGs with Metascape database (L). All data are presented as mean ± SEM. *Significantly different ($p < 0.05$) vs. control group, #significantly different ($p < 0.05$) between groups. (For interpretation of the references to colour in this figure legend, the reader is referred to the web version of this article.)

occurred in arsenic medium- and high-dose group ($p < 0.05$, Fig. 2F).

Meanwhile, hepatic fibrosis-associated genes were screened out based on transcriptome sequencing for identifying the key genes governed the pathophysiological processes of arsenic-induced liver fibrosis. As illustrated in the heatmap of Fig. 2E, the expression of fibrosis-related genes, including transforming growth factor-β1 (*TGFB1*), *SMAD2Z*, actin alpha 2 *(ACTA2)*, collagen type I alpha 1 chain (*COL1A1*), collagen type III alpha 1 chain (*COL3A1*), collagen type IV alpha 1 chain (*COL4A1*), and signal transducer and activator of transcription (STAT) family (*STAT1*, *STAT2*, *STAT3*, and *STAT4*), showed a certain trend of change during 30 mg/L arsenic exposure (Fig. 2E).

Interestingly, dramatical loss of *SIRT6* expression in arsenic-exposed chicken livers was displayed, accompanied by an increase in *SMAD2* expression (Fig. 2G and H). Further western blot was reliably employed for the protein levels of Sirt6 and Smad2, and the trend of the two proteins was consistent with the mRNA levels variation (Fig. 2I and J).

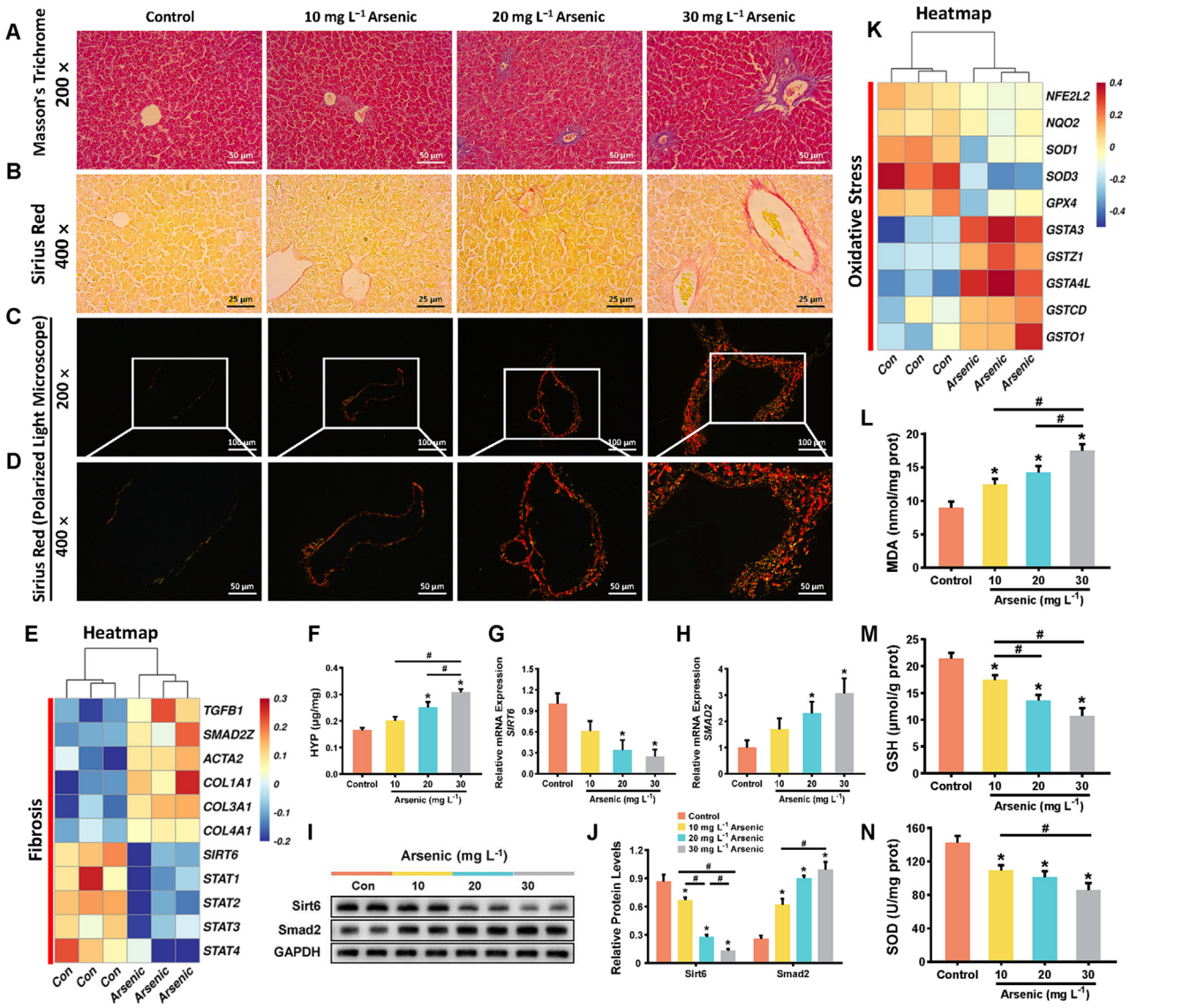

Fig. 2. Arsenic administration induced liver fibrosis and affected redox homeostasis in chickens. Masson's trichrome staining (A) and Sirius red staining under light microscope (B) and polarized light microscope (C-D), respectively, of chicken livers (A: Scale bar = 50 μm, magnification 200 ×; B: Scale bar = 25 μm, magnification 400 ×; C: Scale bar = 100 μm, magnification 200 ×; D: Scale bar = 50 μm, magnification 400 ×). Heatmaps of fibrosis-associated genes expression (E) based on mRNA-sequencing data. Liver tissue HYP content (F) from each group (n = 7). Relative mRNA expression (G and H) and protein levels (I and J) of Sirt6 and Smad2 in chicken livers from each group respectively with western blot (n = 4) and qRT-PCR (n = 5). Heatmaps of redox-associated mRNA expression (K) based on mRNA-sequencing data. Oxidative stress biomarkers MDA concentration (L), GSH level (M), and SOD activity (N) in chicken livers (n = 7). All data are expressed as mean ± SEM. *Significantly different ($p < 0.05$) vs. control group, #significantly different ($p < 0.05$) between groups. (For interpretation of the references to colour in this figure legend, the reader is referred to the web version of this article.)

Arsenic administration induced liver redox imbalance in chickens

As oxidative stress is proven to be one of the pathomechanisms responsible for arsenic exposure, redox-associated mRNA-sequencing data were collected. Vital oxidative stress response genes including nuclear factor-erythroid-2-related factor 2 (*NFE2L2*, a key redox sensitive transcription factor defending against toxic-induced oxidative insults, closely related to lipid homeostasis) [33,40], NAD(P)H quinone dehydrogenase 2 (*NQO2*), superoxide dismutase 1 (*SOD1*), superoxide dismutase 3 (*SOD3*), and glutathione peroxidase 4 (*GPX4*) were down-regulated under 30 mg/L arsenic intervention (Fig. 2K). Meanwhile, we found that the glutathione S-transferase (*GST*) gene family (*GSTA3*, *GSTZ1*, *GSTA4L*, *GSTCD*, *GSTO1*, and *GSTA2*) in response to oxidative stress were mostly up-regulated significantly (Fig. 2K). Furthermore, bio-markers of redox homeostasis were determined. Our data were consistent with our previous investigation of arsenic-induced liver injury in rats [41]. Concretely, the oxidant production MDA was over-accumulated (Fig. 2L), the antioxidant enzyme SOD activity and cellular antioxidant GSH level were down-regulated dose-dependently (Fig. 2M and N), marking the weakening of antioxidant defense. Moreover, the above indexes in chickens upon arsenic treatment showed a significant alteration ($p < 0.05$, Fig. 2-L-N).

Arsenic administration induced liver steatosis, disturbed CHO and BAs synthesis in chickens

Steatosis is regarded as the consequence of moderate to severe hepatocellular insult. Lipid levels in response to biochemical tests were assessed. Arsenic treatment aggravated TG and CHO accumulation in chicken serum, along with a marked increase in the 20 or

30 mg/L arsenic group ($p < 0.05$, Fig. 3B and C). Furthermore, aberrant concentration of HDL and LDL strongly linked to liver disease. The decrease of HDL and the increase of LDL were shown in response to arsenic dose-dependently (Fig. 3D and E). Importantly, TBA levels were high in arsenic-treated chicken serum dose-dependently, with a significant elevation in 20 mg/L and 30 mg/L arsenic-treated group ($p < 0.05$, Fig. 3A).

The heatmap of steatosis-related genes expression including peroxisome proliferator-activated receptor-γ (*PPARG*, a regulator of classic lipid metabolism in adipocytes and hepatocytes) [42,43], fatty acid-binding protein 5 (*FABP5*), fatty acid-binding protein 6 (*FABP6*), peroxisome proliferator-activated receptor-alpha (*PPARA*), acyl-CoA oxidase 1 (*ACOX1*), cluster of differentiation 36 (*CD36*), acetyl-CoA acyltransferase 1 (*ACAA1*), ELOVL fatty acid elongase 6 (*ELOVL6*), fatty acid synthase (*FASN*), and microsomal triglyceride transfer protein (*MTTP*) showed a certain trend of change during 30 mg/L arsenic exposure (Fig. 3F).

Oil Red O staining is regarded as a "gold standard" for specifically recognizing and quantifying lipid droplets. Multiple areas of fat and lipids were caught in frozen sections from arsenic-administrated groups, and the positive area of lipid accumulation increased dose-dependently (Fig. 3J).

Liver sequencing showed significantly changes of CHO- and BA-associated genes including acetyl-CoA acetyltransferase 2 (*ACAT2*), 3-hydroxy-3-methylglutaryl-CoA reductase (*HMGCR*, a key CHO biosynthetic enzyme) [44] sterol regulatory element binding

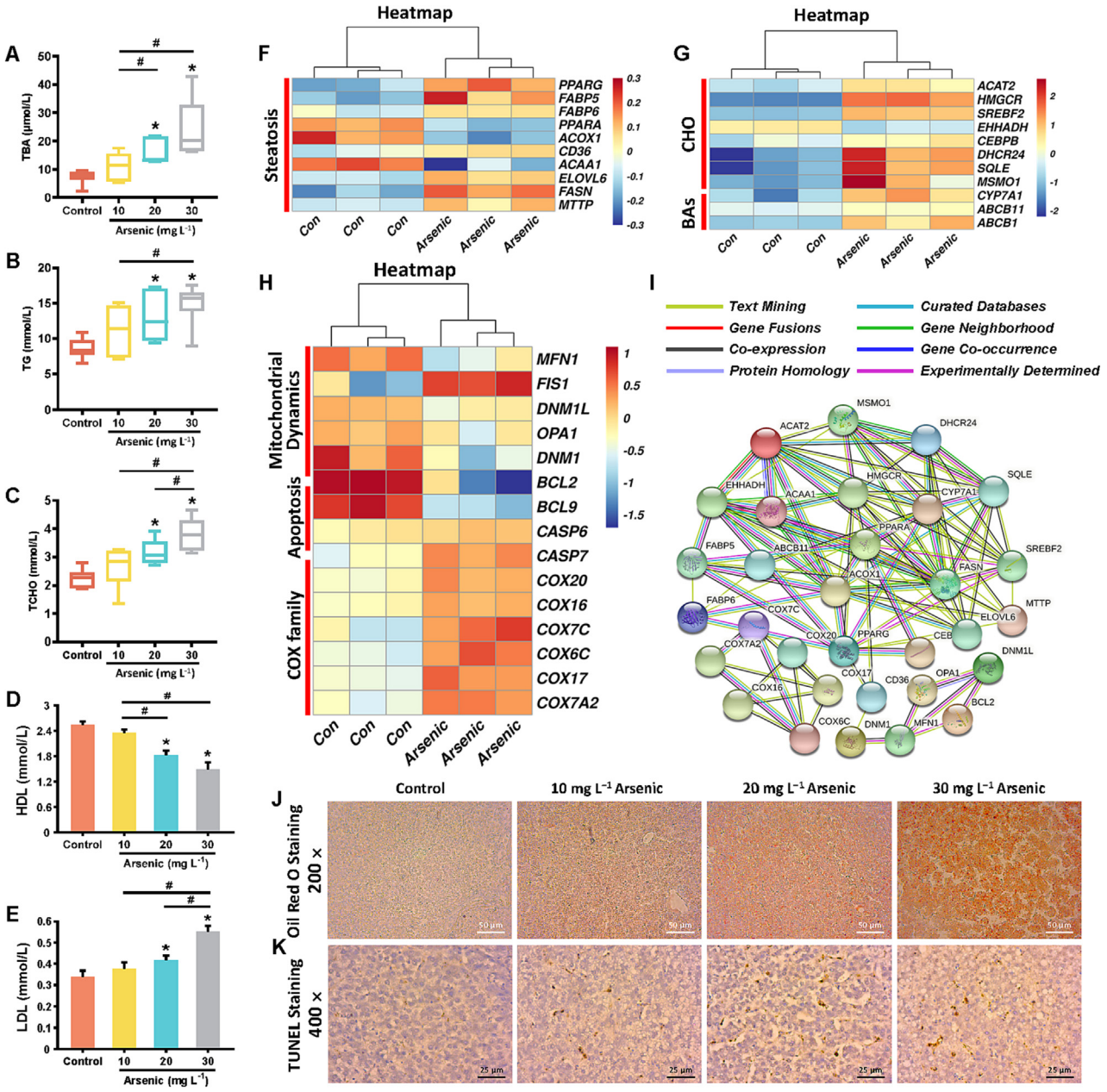

Fig. 3. Arsenic administration caused steatosis, disturbed CHO and BAs synthesis, and induced mitochondrial dynamics disorder and apoptosis in chickens. Serum TBA (A), TG (B), and TCHO (C) contents, HDL (D) and LDL (E) concentration in (n = 7). Heatmaps of steatosis-associated mRNA expression (F), CHO and BAs synthesis-associated mRNA expression (G) based on mRNA-sequencing data. Heatmap (H) of liver mitochondrial dynamics-, apoptosis-, and COX family-associated mRNA expression based on sequencing data. A PPI network (I) of study-related genes. Oil Red O staining (J) presenting areas of lipid accumulation (Scale bar = 50 μm, magnification 200 ×). TUNEL staining (K) in chicken livers (Scale bar = 25 μm, magnification 400 ×). All data are expressed as mean ± SEM. *Significantly different ($p < 0.05$) vs. control group, #significantly different ($p < 0.05$) between groups. (For interpretation of the references to colour in this figure legend, the reader is referred to the web version of this article.)

transcription factor 2 (*SREBF2*, a transcriptional regulator of genes involved in CHO biosynthesis) [45], hydratase/3-hydroxyacyl CoA dehydrogenase (*EHHADA*), CCAAT enhancer binding protein β (*CEBPB*), 24-dehydrocholesterol reductase (*DHCR24*), squalene epoxidase (*SQLE*, a key CHO biosynthetic enzyme) [44], methylsterol monooxygenase 1 (*MSMO1*, a protein coding gene involved in the normal synthesis of CHO) [46], and cytochrome P450 family 7 subfamily A member 1 (*CYP7A1*) in chickens exposed to high-dose arsenic in comparison with the control (Fig. 3G). Furthermore, BAs hepatobiliary transport related genes including ATP-binding cassette subfamily B member 11 (*ABCB11*, the major canalicular transporter of BAs from the hepatocyte) [47,48], and *ABCB1* were also increased in arsenic-exposed liver (Fig. 3G).

Arsenic administration induced mitochondrial dynamics disorder and apoptosis in chickens

Mitochondrial dynamics- and apoptosis-linked key genes were respectively identified. Mitochondrial morphology is determined by the balance between mitochondrial fusion and fission [49]. Liver mitochondrial dynamics disorder was evidenced by the alteration of mitochondrial fusion-related proteins mitofusin 1 (*MFN1*) and mitochondrial dynamin like GTPase (*OPA1*), and mitochondrial fission-related proteins mitochondrial fission 1 protein (*FIS1*), dynamin 1 like (*DNM1L*), and dynamin 1 (*DNM1*) mRNA expression (Fig. 3H).

B-cell lymphoma gene 2 (BCL-2) and BCL-9 are important anti-apoptotic protein [33], caspase 6 (CASP6) and CASP7 are essential executioners acted on substrate cleavage and the destruction of subcellular structures [50,51]. Liver apoptosis was confirmed by the down-regulated *BCL2* and *BCL9* mRNA expression and the up-regulated *CASP6* and *CASP7* mRNA expression (Fig. 3H). Moreover, *in situ* apoptosis detection was accomplished based on the biotin-dUTP labeling and diaminobenzidine (DAB) staining. The proportion of DAB imaging positive cells (brown) from each groups revealed severer apoptosis in arsenic-exposed chicken livers, and it was dose-related (Fig. 3K). Furthermore, we noticed a significant up-regulation in *COX* gene family (Fig. 3H).

PPI analysis

The genes related to arsenic-triggered a serious of lesion in liver were revealed in the PPI network (Fig. 3I). The edges connected different proteins represented known interactions, predicted interactions, and so on.

Arsenic administration induced dramatic gut microbiota remodeling in chicken ilea

In order to interrogate the underlying effect of arsenic in mediating intestinal homeostasis, bacterial 16S rRNA gene sequencing on ileum content from chickens in absence or presence of 30 mg/L arsenic was conducted. As predicted, arsenic administration largely influenced bacterial community alpha diversity indexes as a measure of species diversity, reflected by the dramatical repression of Shannon diversity index, observed OTUs, Pielou's evenness index, and Faith's phylogenetic diversity of ileum microbiota (Fig. 4A-D, $p < 0.05$).

Under the condition of arsenic treatment, the bacterial abundances at diverse levels (phylum, class, order, family, genus, and species) showed an obvious alteration in Fig. 4E and F and Fig. S2. Specifically, arsenic dramatically elevated the ratio of *Firmicutes*/*Bacteroidota* regarding as dysbiosis (Fig. 4G, $p < 0.05$). Linear discriminant analysis Effect Size (LEfSe) was next employed to distinguish the variations of gut microbiota (LDA store > 3) for probing the dominant communities that were characteristic between the control and arsenic-exposed group (Fig. 4H and I). Concurrently, the relative abundance of *Christensenellaceae* (a therapeutic bacterium) and *Muribaculaceae* family (an advantageous bacterial group in *Bacteroidales* order) were significantly repressed under arsenic treatment. Moreover, arsenic exposure dramatically reduced the abundance of *Faecalibacterium* genus and *Ruminococcaceae* family (Fig. 4H and I, $p < 0.05$). Of note, arsenic administration markedly increased the relative abundance of *Proteiniphilum* genus (a Gram-negative bacteria), *Bacilli* order, and *Lactobacillaceae* family (Fig. 4H and I, $p < 0.05$). Taken together, 16S rRNA gene sequencing results of stool samples obviously revealed the drastic changes in gut microbiota induced by arsenic.

Arsenic administration affected intestinal barrier and induced intestinal toxicity in chickens

To further examine the effect of arsenic on intestinal, H&E staining (Fig. 5A) were performed and dramatically presented the noxious effect of arsenic. From the result of histology analysis (Fig. 5A), arsenic treatment showed destructed ileum tissue structure with a significant reduction of villous height (Fig. 5B) and crypt depth (Fig. 5C). Moreover, arsenic supplementation strongly increased the intestinal barrier permeability. Tight junction proteins *CLDN1* and *OCLN* mRNA expression level in ilea were decreased by arsenic administration dose-dependently, so did the zonula occludens-1 (*ZO-1*) level (Fig. 5G). The protein levels of CLDN1 and OCLN were completely consistent with the tendency of qPCR assay, with a markedly decrease in the presence of arsenic (Fig. 5D and E). What's more, the increased intestinal permeability based on the barrier dysfunction is supposed to cause LPS translocation. We evidently noticed a strong elevation of serum LPS levels in arsenic-treated chickens (Fig. 5I). Furthermore, in comparison with the control group, arsenic intervention strongly rose the inflammatory response-related mRNA expression of *NF-κB*, interleukin-1β (*IL-1β*), toll-like receptor 4 (*TLR4*), interferon-γ (*IFN-γ*), and *TNF-α* dose-dependently, meanwhile, decreased the *IL-6* mRNA expression (Fig. 5H). The protein levels of TGF-β1, TNF-α, IL-1β, and NF-κB (nuclear) showed a significant upward trend with the increasing dose of arsenic treatment (Fig. 5D, E, and F).

Correlation analysis of liver-microbiota-gut axis in chickens

As shown in Fig. 5J, Pearson correlation coefficient identified the statistical association between gut microbiota and indexes associated with liver and intestinal injury. *Christensenellaceae*, *Lachnospiraceae*, *Muribaculaceae*, *Ruminococcaceae*, *Faecalibacterium*, and *Lactobacillaceae* highly correlated with intestinal inflammatory, liver function, and liver fibrosis in chickens (Fig. 5J). In Fig. 5K, liver fibrosis indexes, liver function indicators, LPS, intestinal barrier integrity and intestinal inflammatory indices related to this study presented strong correlation (Fig. 5K). Altogether, these results indicate that liver-microbiota-gut axis collectively contributes to the biotoxicity in chickens chronically exposed to arsenic.

Arsenic administration altered serum metabolome in chickens

Serum metabolome was then conducted as a bridge for further interrogating the correlation between gut and liver in chickens. Five serum samples respectively from the control and 30 mg/L arsenic group were analyzed with LC-MS. A total of 323 metabolites were identified. In this study, the criteria for differential metabolite screening were p-value ≤ 0.05 and Variable Importance in Projection ≥ 1. The z-score plot and heatmap of identified differential metabolites in serum revealed a significant statistic difference in expression level of N-Methyl-2-pyrrolidinone, estrone,

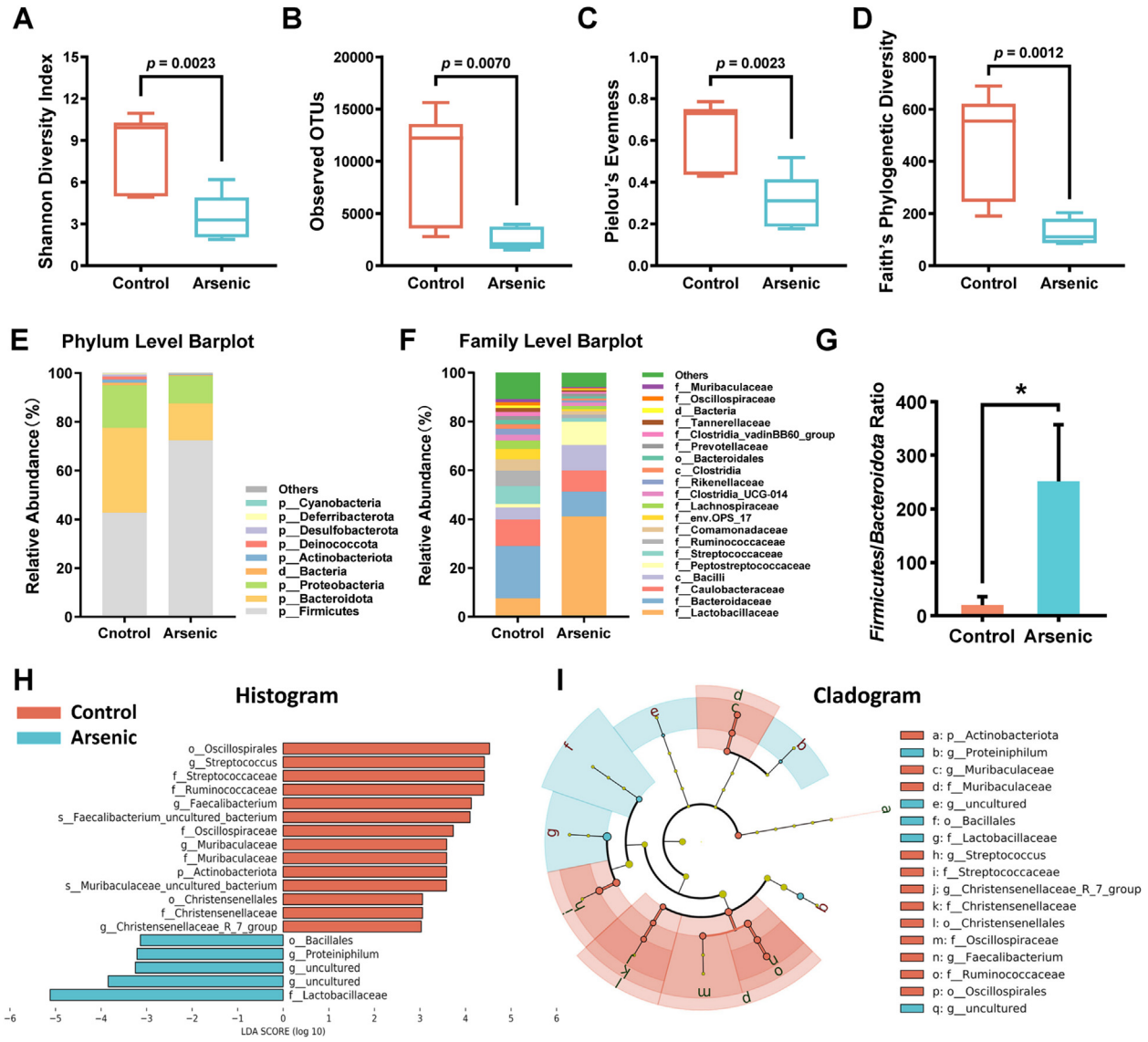

Fig. 4. Arsenic administration disturbed gut microbiota composition in chicken ilea. The Alpha diversity indices boxplot of samples: Shannon diversity index (A), observed OTUs (B), Pielou's evenness index (C), and Faith's phylogenetic diversity (D) of ileum microbiota (n = 9). Relative abundance of different gut bacteria at the phylum (E) and family (F) level (n = 9). The ratio of *Firmicutes*/*Bacteroidota* (G) in chicken ileum microbiota (n = 9). LDA score plot (H) and cladograms plot (I) generated from LEfSe analysis representing multiple taxa differentially enriched in the stool samples from chickens in absence or presence of 30 mg/L arsenic at the LDA threshold of 3.0 (p: Phylum, c: Class, o: Order, f: Family, g: Genus). All data are expressed as mean ± SEM. *Significantly different ($p < 0.05$) vs. control group, #significantly different ($p < 0.05$) between groups.

aminohydroquinone, L-Methionine S-oxide, diacetyl, gamma-Aminobutyric acid, chenodeoxycholic acid (CDCA), L-2,4-diaminobutyric acid, 1H-Indole-3-carboxaldehyde, nicotinic acid, 13S-hydroxyoctadecadienoic acid, phosphonoacetate, Se-Methylselenocysteine, 4-Quinolinecarboxylic acid, methyl jasmonate, and galactaric acid either arsenic treatment or not (Fig. 6A and B). The application of multivariate statistical analysis clearly evaluated the distinction between samples from each group. In this study, the PCA score plot of serum metabolites clearly presented a considerable discrimination either arsenic treatment or not, revealing the distinct separation trend (Fig. 6C). Meanwhile, partial least squares-discriminant analysis (PLS-DA) and orthogonal PLS-DA (OPLS-DA) score plots derived from group comparison showed strong separation between groups (Fig. 6D-G). Accordingly, the metabolome results well confirmed the effect of arsenic in intervening serum metabolic homeostasis, largely causing hepatotoxicity to a certain extent as possibly.

Especially as predicted, the final metabolite of sodium arsenite—dimethylarsinate was found a very marked elevation in chicken serum (Fig. 6H, $p < 0.05$). Moreover, BAs metabolism associated key different metabolites were identified. Increased primary BAs (PBAs) levels as CDCA and glycocholic acid (GCA), and decreased secondary BAs (SBAs) as ursodeoxycholic acid (UDCA) and lithocholic acid (LCA) were displayed (Fig. 6I-L).

Discussion

Increasing evidence has confirmed the risk of arsenic-contaminated underground water in long-term liver disease. Our previous study has found that chronic arsenic exposure may promote HSCs activation in rat liver [41]. Moreover, arsenic has been proven to impair intestinal tract [52]. In this study, biochemical outcome and histopathological changes preliminarily revealed

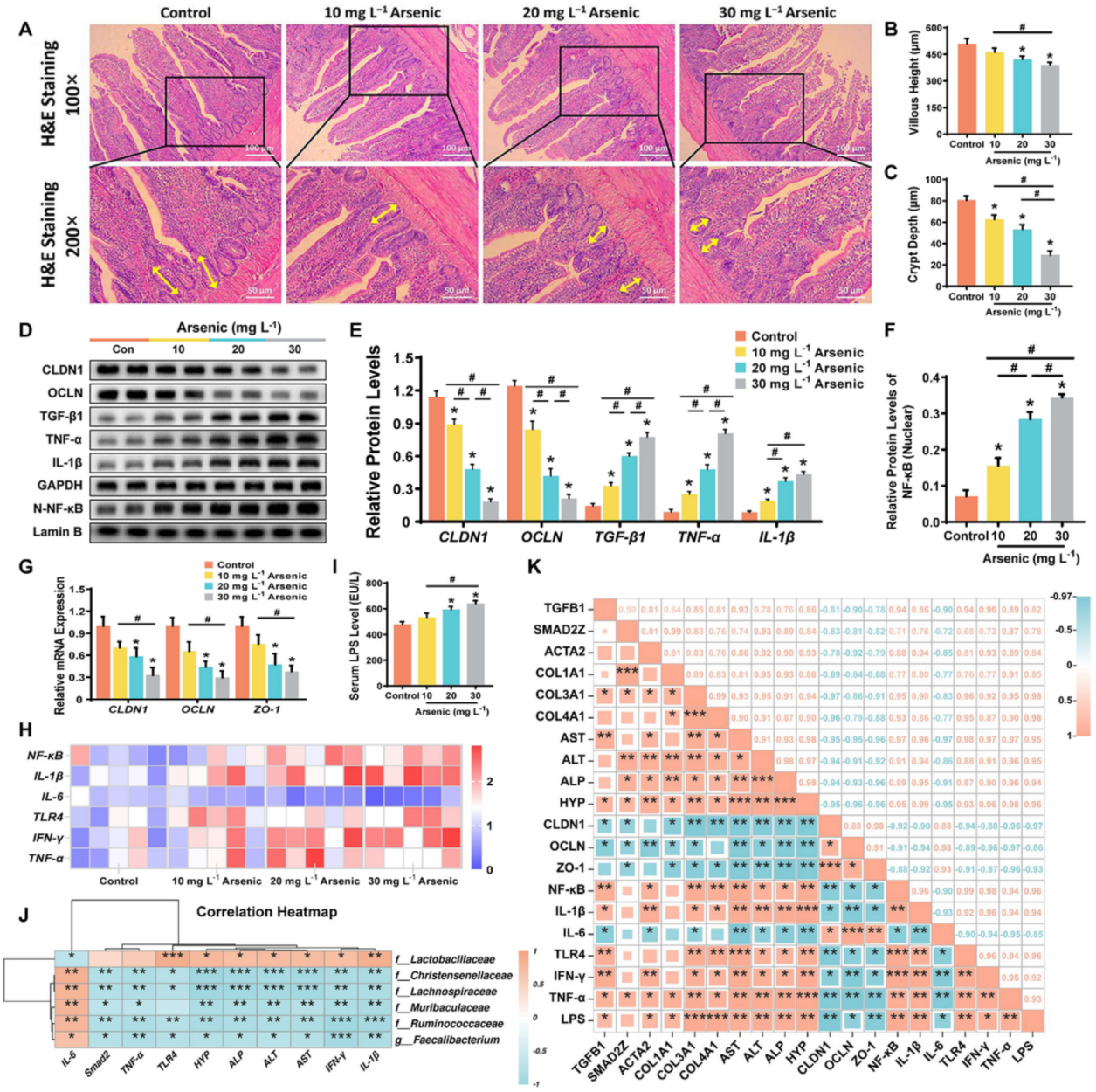

Fig. 5. Arsenic administration induced intestinal injury in chickens. Representative H&E staining images (A) of chicken ilea at 100 × magnification (Scale bar = 100 μm) and 200 × magnification (Scale bar = 50 μm). Yellow double-headed arrows: crypt depth. Villous height (B) and crypt depth (C) in the ilea of chickens treated with/without arsenic (n = 4). The blots (D) and relative protein levels of nuclear NF-κB (F), CLDN1, OCLN, TGF-β1, TNF-α, and IL-1β (E) in chicken ilea (n = 4). Relative mRNA expression of *CLDN1, OCLN, ZO-1* (G) and *NF-κB, IL-1β, IL-6, TLR4, IFN-γ*, and *TNF-α* (H) in chicken ilea (n = 5). Serum LPS level (I) in chickens of each group (n = 7). Correlations (J) between gut microbiota and indexes associated with liver and intestinal injury in chickens determined by Pearson correction analysis. (K) Correlation analysis among liver-microbiota-gut axis. Orange denotes positive correlation and green denotes negative correlation. $^{*}p < 0.05$, $^{**}p < 0.01$, $^{***}p < 0.001$. All data are expressed as mean ± SEM. *Significantly different ($p < 0.05$) vs. control group, #significantly different ($p < 0.05$) between groups. (For interpretation of the references to colour in this figure legend, the reader is referred to the web version of this article.)

the hepatotoxicity of arsenic on chickens, accompanied by an elevation of the final metabolite of sodium arsenite—dimethylarsinate in serum. Furtherly, we found fibrotic lesion, oxidative imbalance, steatosis, inflammation, apoptosis, and mitochondrial dynamics disorder in chicken livers chronically exposed to arsenic, followed by ileal microbiota populations alteration and severe intestinal damage. Here, our present study reveals that chronic arsenic exposure provokes biotoxicity in chickens through disrupting liver-microbiota-gut axis based on multi-omics analysis.

Liver fibrosis is commonly charactered by the *trans*-differentiation effect of activated HSCs [13,53]. Our findings demonstrate the occurrence of pathogenic fibrosis in chicken livers chronically exposed to arsenic preliminarily evidenced by the compelling Sirius red and Masson's trichrome staining, further confirmed by the remarkably elevated transcription levels of hub genes known as fibrosis and HSCs activation. TGF-β1 is a vital pro-fibrogenic factor, essential for the progression of fibrosis [54,55]. TGF-β1 may activate Smad-dependent pathway, drives α-SMA and key ECM genes expression [56]. In this study, arsenic exposure promoted TGF-β1/Smad2 signaling pathway, enhanced α-SMA expression and HSCs activation, ultimately leading to an accumulation of fibrillar collagens. Of note, in the course of data analyzing, we captured a prominent gene, Sirt6, a NAD^{+}-dependent nuclear histone deacetylase, with a marked depletion

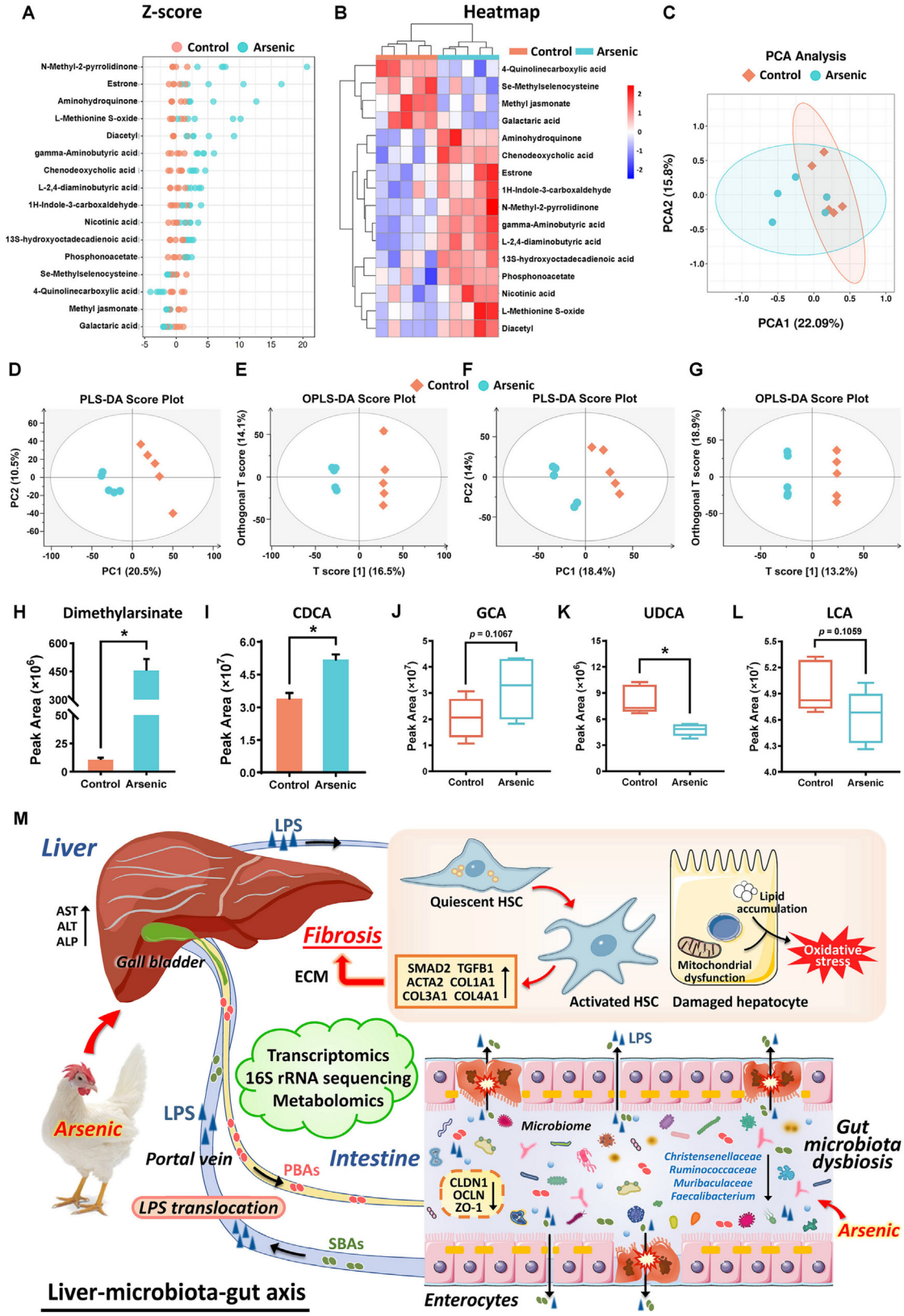

Fig. 6. Arsenic administration induced serum metabolome alteration in chickens. The z-score plot (A) and heatmap (B) of identified differential metabolites in serum of chickens treated with/without arsenic (n = 5). Multivariate statistical analysis based on PCA, PLS-DA, and OPLS-DA analysis. PCA (C) and PLS-DA (D: positive, E: negative) and OPLS-DA (F: positive, G: negative) score plots for the control group vs. 30 mg/L arsenic group in positive and negative ion modes. Associated differential metabolites including dimethylarsinate (H), CDCA (I), GCA (J), UDCA (K), and LCA (L) levels in the serum of control group vs. 30 mg/L arsenic group. Schematic diagram (M) of the arsenic-induced biotoxicity based on multi-omics analysis in chickens. Chronic inorganic arsenic exposure provoked liver-microbiota-gut axis disruption in chickens. All data are expressed as mean ± SEM. *Significantly different ($p < 0.05$) vs. control group.

in arsenic-exposed chicken livers. It was documented that Sirt6 could directly interact with Smad2 and suppress its phosphorylation and nuclear localization in HSCs, further alleviate fibrosis through classical TGF-β1/Smad pathway [57]. Herein, we briefly speculated that Sirt6 depletion may possibly involve in arsenic-induced liver fibrosis and HSCs activation in chickens, and associated molecular mechanisms need further investigation. Hence, our findings indicate that chronic arsenic exposure strongly contributes to liver fibrosis via HSCs activation in chickens.

Intestinal barrier dysfunction and microbiotas dysbiosis have emerged as promising candidates for a wide range of diseases, especially hepatic disorder [58]. In this study, failure of the intestinal tissue integrity exhibited in arsenic-administrated chicken ilea, involved in the down-expression of tight junction-associated proteins, which may cause nearly one hundred trillion microbes invading body as pathogens. Meanwhile, the pathogenic role of intestinal barrier dysfunction usually complicates with chronic intestinal inflammation. The marked alteration of inflammatory factors confirmed the intestinal inflammation evoked by arsenic exposure in our present study. Thus, our findings jointly demonstrate the exact lesion of chronic arsenic exposure to intestinal barrier dysfunction in chickens.

Upon the impairment of intestinal barrier, the raised intestinal permeability allows several pathogen-associated molecular patterns (PAMPs) diverting to the blood, finally releasing to invade tissues and organs [17,59]. LPS is a well-known PAMP anchored in the outer double-membrane envelope of Gram-negative bacteria (as *Proteiniphilum*) driving multiple inflammatory cytokines in response to infections [60–63]. Our study indicates that chronic arsenic exposure contributes to the release of noxious LPS into the circulation, which is supported by the accumulation of LPS in chicken serum. And this process largely depends on portal vein circulation, which acts on manipulating mostly blood from digestive tract directly emptying into the liver, functionally connecting the liver and gut [16]. Accumulating evidence point out that LPS is strongly associated with liver dysfunction and acts as a hepatic endotoxin contributing to diversified liver injury [64,65]. Furthermore, LPS stimulation has been proven to mediate HSCs activation inducing liver fibrosis [66]. In this study, we found the elevated liver function-associated enzyme activities, obvious fibrotic lesion, and the over-expressed of HSCs activation markers in chickens chronically exposed to arsenic. Hence, our results suggest that chronic arsenic exposure triggers enterogenous LPS translocation into liver, leading to a series of hepatic injury in chickens, especially liver fibrosis.

The liver communicates back to the intestine by hepatic bile flow and other mediators, which forms a typical enterohepatic circulation model [17,67]. BAs homeostasis is tightly mediated by enterohepatic signaling [68,69]. Referring to our results of liver transcriptomics and serum metabonomics, we found a severe disturbance in BAs anabolism. CYP7A1 is a key rate-limiting enzyme, responsible for initiating the classic pathway of BAs synthesis [70]. In our study, arsenic exposure significantly up-regulated the *CYP7A1* expression in chicken livers, inducing excessive serum TBA accumulation, which resulted in intestinal epithelial damage. It is well known that hepatocytes synthesize CHO catabolism production PBAs such as CDCA. PBAs subsequently transport into the intestine, convert to SBAs under the action of gut bacteria, further recirculate to the liver via enterohepatic circulation [18,71]. Hence, our current results suggest that arsenic exposure massively increases the concentration of serum PBAs—CDCA and GCA in chickens. Additionally, *Lactobacillaceae*, considered as a beneficial bacterium with CHO-lowering capacity, was found enriched in chicken ilea under arsenic exposure, which is contrary to general studies. We speculate that the elevation of *Lactobacillaceae* abundance could be a positive response process for organism, in turn leads to the decrease percentage of other beneficial bacteria, which directly affects intestinal function of chickens chronically exposed to arsenic.

Our study also identified a strong correlation between SBAs metabolism and several differentially abundant microbes in arsenic-exposed chicken ilea. It is worth noting that only few recognized microbes from *Ruminococcaceae* and *Lachnospiraceae* families have the capacity to dehydroxylate the subsequent 7α of cholic acid (CA) and CDCA in generating classical SBAs [72]. In the present study, arsenic exposure repressed the concentration of several SBAs, especially the LCA and UDCA, in chicken serum, which is involved in the repressed dehydroxylation of *Ruminococcaceae* and *Lachnospiraceae* families in ilea to a certain extent. Furthermore, the reduced abundance of *Ruminococcaceae* has been found in non-alcoholic steatohepatitis [73], indicating the compelling associations between intestinal flora and hepatic disease. Sinha et al. (2020) has also announced the depletion of *Ruminococcaceae* and stool SBAs reduction in patients with ulcerative colitis, simultaneously confirmed the effectiveness of LCA supplementation in alleviating inflammation [74]. Therefore, our findings convincingly elucidate the adverse effect of chronic arsenic exposure on BAs metabolism in chickens, which largely associated with the alteration of enterohepatic circulation of BAs, eventually aggravating liver and intestine damage.

The depleted abundance of profitable microbiota is commonly related to intestinal injury. We further focused on several potentially beneficial gut microbes showing strong negative relevance with arsenic-induced enterohepatic toxicity in chickens. In the present study, the depleted abundance of microbiota including *Christensenellaceae*, *Muribaculaceae*, *Faecalibacterium*, and *Ruminococcaceae* from chicken ilea were observed in the presence of arsenic. Among them, *Christensenellaceae* is known to negatively correlate with serum lipids, metabolic syndrome, and inflammation [75,76]. *Muribaculaceae* also negatively correlates with inflammation status and is beneficial to intestinal epithelial health [77,78]. *Faecalibacterium* is generally regarded as an organism with superior metabolic capacities and showed a reduction under chronic pathological conditions as non-alcoholic fatty liver disease [79,80]. Besides, *Ruminococcaceae* and *Faecalibacterium prausnitzii* (the only species isolated from *Faecalibacterium* genus) were confirmed to be inversely correlated with fibrosis severity in several studies [73,81], which further strongly consistent with the findings of arsenic-induced liver fibrosis in this study. Consequently, these findings collectively corroborate the adverse impact of chronic arsenic exposure on liver-microbiota-gut axis in chickens (Fig. 6M).

Conclusion

In summary, our study established a novel mechanism for comprehensively interpreting the toxicological effect and mechanism of inorganic arsenic exposure in chickens based on integrated multi-omics analysis. Chronic arsenic exposure induced a serious of chicken liver dysfunction, especially severe liver fibrosis, altered ileal microbiota diversity, accompanied by a depletion of potentially beneficial microbes, *Christensenellaceae*, *Ruminococcaceae*, *Muribaculaceae*, and *Faecalibacterium*, simultaneously impaired chicken intestinal barrier integrity, further drove enterogenous LPS translocation aggravating liver toxicity. Moreover, the injured liver negatively intervened BAs homoeostasis, which in turn promoted intestinal injury, ultimately perpetuating pernicious circle. The liver-microbiota-gut axis may become potential therapeutic targets for arsenic-induced systemic toxicity in poultry. Restoring intestinal microbiota balance such as fecal microbiota transplantation to stabilize hepatointestinal microenvironment may be a feasible scheme for preventing environmental arsenic poisoning, and

further studies are warranted to conduct prospective clinical trial for assessing the effectiveness of probiotics in restoring body health.

CRediT authorship contribution statement

Jiayi Li: Conceptualization, Methodology, Validation, Software, Data curation, Writing – original draft. **Changming Guo:** Conceptualization, Validation, Formal analysis, Methodology. **Yan Liu:** Conceptualization, Methodology, Software, Data curation. **Biqi Han:** Conceptualization, Methodology, Software, Data curation, Validation. **Zhanjun Lv:** Methodology, Software, Validation. **Huijie Jiang:** Software, Formal analysis, Validation. **Siyu Li:** Data curation, Validation. **Zhigang Zhang:** Conceptualization, Methodology, Supervision, Writing – review & editing, Project administration.

Declaration of competing interest

The authors declare that they have no known competing financial interests or personal relationships that could have appeared to influence the work reported in this paper.

Acknowledgements

This study was supported by Scientific Research Foundation for the Returned Overseas Chinese Scholars of Heilongjiang Province [grant numbers LC2017007] and the National Natural Science Foundation of China [grant numbers 31972754]. All authors are grateful to E-GENE Technology Co., Ltd (Shenzhen, China) for the sequencing and technical support in the experimental process.

Compliance with Ethics Requirements

All Institutional and National Guidelines for the care and use of animals (fisheries) were followed. All animal experiments were performed in accordance with the Ethical Committee for Animal Experiments of Northeast Agricultural University. The ethical committee number for the study is 202104118.

Appendix A. Supplementary material

Supplementary data to this article can be found online at https://doi.org/10.1016/j.jare.2024.01.019.

References

[1] United States Agency for Toxic Substances and Diseases Registry (ATSDR), Toxicological profile for arsenic, (2007) Available from: https://www.atsdr.cdc.gov/spl/resources/2007_atsdr_substance_priority_list.html.
[2] Podgorski J, Berg M. Global threat of arsenic in groundwater. Science 2020;368:845–50. doi: https://doi.org/10.1126/science.aba1510.
[3] Zhang L, Gao Y, Wu SL, Zhang SQ, Smith KR, Yao XH, et al. Global impact of atmospheric arsenic on health risk: 2005 to 2015. Proc Natl Acad Sci U.S.A. 2020;117:13975–82. doi: https://doi.org/10.1073/pnas.2002580117.
[4] Rahman M, Sohel N, Yunus FM, Alam N, Nahar Q, Streatfield PK, et al. Arsenic exposure and young adult's mortality risk: A 13-year follow-up study in Matlab, Bangladesh. Environ Int 2019;123:358–67. doi: https://doi.org/10.1016/j.envint.2018.12.006.
[5] Bhowmick S, Pramanik S, Singh P, Mondal P, Chatterjee D, Nriagu J. Arsenic in groundwater of West Bengal, India: A review of human health risks and assessment of possible intervention options. Sci Total Environ 2018;612:148–69. doi: https://doi.org/10.1016/j.scitotenv.2017.08.216.
[6] Kumar S, Choudhary AK, Suyal DC, Makarana G, Goel R. Leveraging arsenic resistant plant growth-promoting rhizobacteria for arsenic abatement in crops. J Hazard Mater 2022;425:. doi: https://doi.org/10.1016/j.jhazmat.2021.127965127965.
[7] United States Environmental Protection Agency (US EPA), Drinking water standard for arsenic, (2001) Available from: https://www.epa.gov/dwreginfo/drinking-water-arsenic-rule-history/ (accessed 17 March 2021).
[8] Li LZ, Bi ZY, Wadgaonkar P, Lu YJ, Zhang Q, Fu Y, et al. Metabolic and epigenetic reprogramming in the arsenic-induced cancer stem cells. Semin Cancer Biol 2019;57:10–8. doi: https://doi.org/10.1016/j.semcancer.2019.04.003.
[9] Cuykx M, Rodrigues RM, Laukens K, Vanhaecke T, Covaci A. In vitro assessment of hepatotoxicity by metabolomics: A review. Arch Toxicol 2018;92:3007–29. doi: https://doi.org/10.1007/s00204-018-2286-9.
[10] Zheng SL, Yang Y, Wen C, Liu WY, Cao LH, Feng XL, et al. Effects of environmental contaminants in water resources on nonalcoholic fatty liver disease. Environ Int 2021;154:. doi: https://doi.org/10.1016/j.envint.2021.106555106555.
[11] Xu M, Xu HH, Lin Y, Sun XN, Wang LJ, Fang ZP, et al. LECT2, a ligand for Tie1, plays a crucial role in liver fibrogenesis. Cell 2019;178:1478–1492.e20. doi: https://doi.org/10.1016/j.cell.2019.07.021.
[12] Tsochatzis EA, Bosch J, Burroughs AK. Liver cirrhosis. Lancet 2014;383:1749–61. doi: https://doi.org/10.1016/S0140-6736(14)60121-5.
[13] Tsuchida T, Friedman SL. Mechanisms of hepatic stellate cell activation. Nat Rev Gastroenterol Hepatol 2017;14:397–411. doi: https://doi.org/10.1038/nrgastro.2017.38.
[14] Sun J, Shi L, Xiao T, Xue JC, Li JJ, Wang PW, et al. microRNA-21, via the HIF-1α/VEGF signaling pathway, is involved in arsenite-induced hepatic fibrosis through aberrant cross-talk of hepatocytes and hepatic stellate cells. Chemosphere 2021;266:. doi: https://doi.org/10.1016/j.chemosphere.2020.129177129177.
[15] Kim SW, Less JF, Wang L, Yan T, Kiron V, Kaushik SJ, et al. Meeting global feed protein demand: Challenge, opportunity, and strategy. Annu Rev Anim Biosci 2019;7:221–43. doi: https://doi.org/10.1146/annurev-animal-030117-014838.
[16] Albillos A, de Gottardi A, Rescigno M. The gut-liver axis in liver disease: Pathophysiological basis for therapy. J Hepatol 2020;72:558–77. doi: https://doi.org/10.1016/j.jhep.2019.10.003.
[17] Tripathi A, Debelius J, Brenner DA, Karin M, Loomba R, Schnabl B, et al. The gut-liver axis and the intersection with the microbiome. Nat Rev Gastroenterol Hepatol 2018;15:397–411. doi: https://doi.org/10.1038/s41575-018-0011-z.
[18] Li TG, Chiang JYL. Bile acid signaling in metabolic disease and drug therapy. Pharmacol Rev 2014;66:948–83. doi: https://doi.org/10.1124/pr.113.008201.
[19] Perino A, Demagny H, Velazquez-Villegas L, Schoonjans K. Molecular physiology of bile acid signaling in health, disease, and aging. Physiol Rev 2021;101:683–731. doi: https://doi.org/10.1152/physrev.00049.2019.
[20] Naraharisetti SB, Aggarwal M, Ranganathan V, Sarkar SN, Kataria M, Malik JK. Effects of simultaneous repeated exposure at high levels of arsenic and malathion on hepatic drug-biotransforming enzymes in broiler chickens. Environ Toxicol Pharmacol 2009;28:213–8. doi: https://doi.org/10.1016/j.etap.2009.04.006.
[21] Patel B, Das R, Gautam A, Tiwari M, Acharya S, Kumar S. Evaluation of vascular effect of arsenic using in vivo assays. Environ Sci Pollut Res Int 2017;24:15521–7. doi: https://doi.org/10.1007/s11356-017-9156-5.
[22] Han B, Li SY, Lv YY, Yang DQ, Li JY, Yang QY, et al. Dietary melatonin attenuates chromium-induced lung injury via activating the Sirt1/Pgc-1α/Nrf2 pathway. Food Funct 2019;10:5555–65. doi: https://doi.org/10.1039/c9fo01152h.
[23] Li D, Ji SY, Guo YQ, Sang N. Ambient NO_2 exposure sex-specifically impairs myelin and contributes to anxiety and depression-like behaviors of C57BL/6J mice. J Hazard Mater 2021;416:. doi: https://doi.org/10.1016/j.jhazmat.2021.125836125836.
[24] Han BQ, Li JY, Li SY, Liu Y, Zhang ZG. Effects of thiacloprid exposure on microbiota-gut-liver axis: Multiomics mechanistic analysis in Japanese quails. J Hazard Mater 2023;442:. doi: https://doi.org/10.1016/j.jhazmat.2022.130082130082.
[25] Li JY, Jiang HJ, Wu PF, Li SY, Han B, Yang QY, et al. Toxicological effects of deltamethrin on quail cerebrum: Weakened antioxidant defense and enhanced apoptosis. Environ Pollut 2021;286:. doi: https://doi.org/10.1016/j.envpol.2021.117319117319.
[26] Han B, Lv ZJ, Zhang XY, Lv YY, Li SY, Wu PF, et al. Deltamethrin induces liver fibrosis in quails via activation of the TGF-β1/Smad signaling pathway. Environ Pollut 2020;259:. doi: https://doi.org/10.1016/j.envpol.2019.113870113870.
[27] Hu Q, Liu C, Zhang D, Wang R, Qin LL, Xu Q, et al. Effects of low-dose antibiotics on gut immunity and antibiotic resistomes in weaned piglets. Front Immunol 2020;11:903. doi: https://doi.org/10.3389/fimmu.2020.00903.
[28] Zhou YY, Zhou B, Pache L, Chang M, Khodabakhshi AH, Tanaseichuk O, et al. Metascape provides a biologist-oriented resource for the analysis of systems-level datasets. Nat Commun 2019;10:1523. doi: https://doi.org/10.1038/s41467-019-09234-6.
[29] Ren L, Wang G, Huang YX, Guo JF, Li CY, Jia Y, et al. Phthalic acid esters degradation by a novel marine bacterial strain *Mycolicibacterium phocaicum* RL-HY01: Characterization, metabolic pathway and bioaugmentation. Sci Total Environ 2021;791:. doi: https://doi.org/10.1016/j.scitotenv.2021.148303148303.
[30] Zhang CY, Hu ZS, Hu RM, Pi SX, Wei ZJ, Wang C, et al. New insights into crosstalk between pyroptosis and autophagy co-induced by molybdenum and cadmium in duck renal tubular epithelial cells. J Hazard Mater 2021;416:. doi: https://doi.org/10.1016/j.jhazmat.2021.126138126138.
[31] Han BQ, Lv ZJ, Han XM, Li SY, Han B, Yang QY, et al. Harmful effects of inorganic mercury exposure on kidney cells: Mitochondrial dynamics disorder and excessive oxidative stress. Biol Trace Elem Res 2022;200:1591–7. doi: https://doi.org/10.1007/s12011-021-02766-3.
[32] Liu BY, Bing QZ, Li SY, Han B, Lu JJ, Baiyun RQ, et al. Role of A_{2B} adenosine receptor-dependent adenosine signaling in multi-walled carbon nanotube-

triggered lung fibrosis in mice. J Nanobiotechnol 2019;17:45. doi: https://doi.org/10.1186/s12951-019-0478-y.
[33] Li JY, Yu ZX, Han B, Li SY, Lv YY, Wang XQ, et al. Activation of the GPX4/TLR4 signaling pathway participates in the alleviation of selenium yeast on deltamethrin-provoked cerebrum injury in quails. Mol Neurobiol 2022;59:2946–61. doi: https://doi.org/10.1007/s12035-022-02744-3.
[34] Li NY, Ansari AR, Sun ZJ, Huang HB, Cui L, Hu YF, et al. Toll like receptor 4 signaling pathway participated in Salmonella lipopolysaccharide-induced spleen injury in young chicks. Microb Pathog 2017;112:288–94. doi: https://doi.org/10.1016/j.micpath.2017.10.004.
[35] Yu L, Lv ZJ, Li SY, Jiang HJ, Han BQ, Zheng XY, et al. Chronic arsenic exposure induces ferroptosis via enhancing ferritinophagy in chicken livers. Sci Total Environ 2023;890:. doi: https://doi.org/10.1016/j.scitotenv.2023.164172164172.
[36] Yang DQ, Tan X, Lv ZJ, Liu BY, Baiyun RQ, Lu JJ, et al. Regulation of Sirt1/Nrf2/TNF-α signaling pathway by luteolin is critical to attenuate acute mercuric chloride exposure induced hepatotoxicity. Sci Rep 2016;6:37157. doi: https://doi.org/10.1038/srep37157.
[37] Li JY, Zheng XY, Ma XY, Xu XY, Du Y, Lv QJ, et al. Melatonin protects against chromium(VI)-induced cardiac injury via activating the AMPK/Nrf2 pathway. J Inorg Biochem 2019;197:. doi: https://doi.org/10.1016/j.jinorgbio.2019.110698110698.
[38] Yang QY, Han B, Li SY, Wang XQ, Wu PF, Liu Y, et al. The link between deacetylation and hepatotoxicity induced by exposure to hexavalent chromium. J Adv Res 2021;35:129–40. doi: https://doi.org/10.1016/j.jare.2021.04.002.
[39] Han B, Wang XQ, Wu PF, Jiang HJ, Yang QY, Li SY, et al. Pulmonary inflammatory and fibrogenic response induced by graphitized multi-walled carbon nanotube involved in cGAS-STING signaling pathway. J Hazard Mater 2021;417:. doi: https://doi.org/10.1016/j.jhazmat.2021.125984125984.
[40] Hayes JD, Dinkova-Kostova AT. The Nrf2 regulatory network provides an interface between redox and intermediary metabolism. Trends Biochem Sci 2014;39:199–218. doi: https://doi.org/10.1016/j.tibs.2014.02.002.
[41] Zhang ZG, Guo CM, Jiang HJ, Han B, Wang XQ, Li SY, et al. Inflammation response after the cessation of chronic arsenic exposure and post-treatment of natural astaxanthin in liver: Potential role of cytokine-mediated cell-cell interactions. Food Funct 2020;11:9252–62. doi: https://doi.org/10.1039/d0fo01223h.
[42] Souza-Mello V. Peroxisome proliferator-activated receptors as targets to treat non-alcoholic fatty liver disease. World J Hepatol 2015;7:1012–9. doi: https://doi.org/10.4254/wjh.v7.i8.1012.
[43] Pi J. Deficiency in the nuclear factor E2-related factor-2 transcription factor results in impaired adipogenesis and protects against diet-induced obesity. J Biol Chem 2010;285:9292–300. doi: https://doi.org/10.1074/jbc.M109.093955.
[44] Gao SS, Soares F, Wang SY, Wong CC, Chen HR, Yang ZJ, et al. CRISPR screens identify cholesterol biosynthesis as a therapeutic target on stemness and drug resistance of colon cancer. Oncogene 2021;40:6601–13. doi: https://doi.org/10.1038/s41388-021-01882-7.
[45] Bommer GT, MacDougald OA. Regulation of lipid homeostasis by the bifunctional SREBF2-miR33a locus. Cell Metab 2011;13:241–7. doi: https://doi.org/10.1016/j.cmet.2011.02.004.
[46] Cao RX, Zhang ZQ, Tian C, Sheng WW, Dong Q, Dong M. Down-regulation of MSMO1 promotes the development and progression of pancreatic cancer. J Cancer 2022;13:3013–21. doi: https://doi.org/10.7150/jca.73112.
[47] Gerloff T, Stieger B, Hagenbuch B, Madon J, Landmann L, Roth J, et al. The sister of P-glycoprotein represents the canalicular bile salt export pump of mammalian liver. J Biol Chem 1998;273:10046–50. doi: https://doi.org/10.1074/jbc.273.16.10046.
[48] Green RM, Hoda F, Ward KL. Molecular cloning and characterization of the murine bile salt export pump. Gene 2000;241:117–23. doi: https://doi.org/10.1016/s0378-1119(99)00460-6.
[49] Cho HM, Sun W. Molecular cross talk among the components of the regulatory machinery of mitochondrial structure and quality control. Exp Mol Med 2020;52:730–7. doi: https://doi.org/10.1038/s12276-020-0434-9.
[50] McIlwain DR, Berger T, Mak TW. Caspase functions in cell death and disease: Figure 1. Cold Spring Harb Perspect Biol 2015;7:. doi: https://doi.org/10.1101/cshperspect.a026716a026716.
[51] Galluzzi L, Lopez-Soto A, Kumar S, Kroemer G. Caspases connect cell-death signaling to organismal homeostasis. Immunity 2016;44:221–31. doi: https://doi.org/10.1016/j.immuni.2016.01.020.
[52] Chiocchetti GM, Vélez D, Devesa V. Inorganic arsenic causes intestinal barrier disruption. Metallomics 2019;11:1411–8. doi: https://doi.org/10.1039/c9mt00144a.
[53] Lin CY, Adhikary P, Cheng K. Cellular protein markers, therapeutics, and drug delivery strategies in the treatment of diabetes-associated liver fibrosis. Adv Drug Deliv Rev 2021;174:127–39. doi: https://doi.org/10.1016/j.addr.2021.04.008.
[54] Lv YY, Bing QZ, Lv ZJ, Xue JD, Li SY, Han B, et al. Imidacloprid-induced liver fibrosis in quails via activation of the TGF-β1/Smad pathway. Sci Total Environ 2020;705:. doi: https://doi.org/10.1016/j.scitotenv.2019.135915135915.
[55] Zhang TZ, He XL, Caldwell L, Goru SK, Ulloa Severino L, Tolosa MF, et al. NUAK1 promotes organ fibrosis via YAP and TGF-β/SMAD signaling. Sci Transl Med 2022;14:eaaz4028. doi: https://doi.org/10.1126/scitranslmed.aaz4028.
[56] Parola M, Pinzani M. Liver fibrosis: Pathophysiology, pathogenetic targets and clinical issues. Mol Aspects Med 2019;65:37–55. doi: https://doi.org/10.1016/j.mam.2018.09.002.
[57] Zhang JH, Li YP, Liu QH, Huang Y, Li R, Wu T, et al. Sirt6 alleviated liver fibrosis by deacetylating conserved lysine 54 on Smad2 in hepatic stellate cells. Hepatology 2021;73:1140–57. doi: https://doi.org/10.1002/hep.31418.
[58] Chopyk DM, Grakoui A. Contribution of the intestinal microbiome and gut barrier to hepatic disorders. Gastroenterology 2020;159:849–63. doi: https://doi.org/10.1053/j.gastro.2020.04.077.
[59] Nakamoto N, Sasaki N, Aoki R, Miyamoto K, Suda W, Teratani T, et al. Gut pathobionts underlie intestinal barrier dysfunction and liver T helper 17 cell immune response in primary sclerosing cholangitis. Nat Microbiol 2019;4:492–503. doi: https://doi.org/10.1038/s41564-018-0333-1.
[60] Borovikova LV, Ivanova S, Zhang M, Yang H, Botchkina GI, Watkins LR, et al. Vagus nerve stimulation attenuates the systemic inflammatory response to endotoxin. Nature 2000;405:458–62. doi: https://doi.org/10.1038/35013070.
[61] Simpson BW, Trent MS. Pushing the envelope: LPS modifications and their consequences. Nat Rev Microbiol 2019;17:403–16. doi: https://doi.org/10.1038/s41579-019-0201-x.
[62] Wu XT, Ansari AR, Pang XX, Li HZ, Zhang ZW, Luo Y, et al. Visfatin plays a significant role in alleviating lipopolysaccharide-induced apoptosis and autophagy through PI3K/AKT signaling pathway during acute lung injury in mice. Arch Immunol Ther Exp 2019;67:249–61. doi: https://doi.org/10.1007/s00005-019-00544-7.
[63] Luo Y, Pang XX, Ansari AR, Wu XT, Li HZ, Zhang ZW, et al. Visfatin exerts immunotherapeutic effects in lipopolysaccharide-induced acute lung injury in murine model. Inflammation 2020;43:109–22. doi: https://doi.org/10.1007/s10753-019-01100-3.
[64] Ashraf KU, Nygaard R, Vickery ON, Erramilli SK, Herrera CM, McConville TH, et al. Structural basis of lipopolysaccharide maturation by the O-antigen ligase. Nature 2022;604:371–6. doi: https://doi.org/10.1038/s41586-022-04555-x.
[65] Szabo G. Gut-liver axis in alcoholic liver disease. Gastroenterology 2015;148:30–6. doi: https://doi.org/10.1053/j.gastro.2014.10.042.
[66] Inzaugarat ME, Johnson CD, Holtmann TM, McGeough MD, Trautwein C, Papouchado BG, et al. NLR family pyrin domain-containing 3 inflammasome activation in hepatic stellate cells induces liver fibrosis in mice. Hepatology 2019;69:845–59. doi: https://doi.org/10.1002/hep.30252.
[67] Tranah TH, Edwards LA, Schnabl B, Shawcross DL. Targeting the gut-liver-immune axis to treat cirrhosis. Gut 2021;70:982–94. doi: https://doi.org/10.1136/gutjnl-2020-320786.
[68] Fuchs CD, Trauner M. Role of bile acids and their receptors in gastrointestinal and hepatic pathophysiology. Nat Rev Gastroenterol Hepatol 2022;19:432–50. doi: https://doi.org/10.1038/s41575-021-00566-7.
[69] Lang S, Schnabl B. Microbiota and fatty liver disease-the known, the unknown, and the future. Cell Host Microbe 2020;28:233–44. doi: https://doi.org/10.1016/j.chom.2020.07.007.
[70] Rizzolo D, Kong B, Taylor RE, Brinker A, Goedken M, Buckley B, et al. Bile acid homeostasis in female mice deficient in Cyp7a1 and Cyp27a1. Acta Pharm Sin B 2021;11:3847–56. doi: https://doi.org/10.1016/j.apsb.2021.05.023.
[71] Sun LL, Pang YY, Wang XM, Wu Q, Liu HY, Liu B, et al. Ablation of gut microbiota alleviates obesity-induced hepatic steatosis and glucose intolerance by modulating bile acid metabolism in hamsters. Acta Pharm Sin B 2019;9:702–10. doi: https://doi.org/10.1016/j.apsb.2019.02.004.
[72] Stellwag EJ, Hylemon PB. 7alpha-Dehydroxylation of cholic acid and chenodeoxycholic acid by Clostridium leptum. J Lipid Res 1979;20:325–33.
[73] Lee G, You HJ, Bajaj JS, Joo SK, Yu J, Park S, et al. Distinct signatures of gut microbiome and metabolites associated with significant fibrosis in non-obese NAFLD. Nat Commun 2020;11:4982. doi: https://doi.org/10.1038/s41467-020-18754-5.
[74] Sinha SR, Haileselassie Y, Nguyen LP, Tropini C, Wang M, Becker LS, et al. Dysbiosis-induced secondary bile acid deficiency promotes intestinal inflammation. Cell Host Microbe 2020;27:659–670.e5. doi: https://doi.org/10.1016/j.chom.2020.01.021.
[75] Jing YL, Yu Y, Bai F, Wang LM, Yang DG, Zhang C, et al. Effect of fecal microbiota transplantation on neurological restoration in a spinal cord injury mouse model: Involvement of brain-gut axis. Microbiome 2021;9:59. doi: https://doi.org/10.1186/s40168-021-01007-y.
[76] Waters JL, Ley RE. The human gut bacteria *Christensenellaceae* are widespread, heritable, and associated with health. BMC Biol 2019;17:83. doi: https://doi.org/10.1186/s12915-019-0699-4.
[77] Liang HY, Song H, Zhang XJ, Song GF, Wang YZ, Ding XF, et al. Metformin attenuated sepsis-related liver injury by modulating gut microbiota. Emerg Microbes Infect 2022;11:815–28. doi: https://doi.org/10.1080/22221751.2022.2045876.
[78] Tian BM, Zhao JH, Zhang M, Chen ZF, Ma QY, Liu HC, et al. *Lycium ruthenicum* anthocyanins attenuate high-fat diet-induced colonic barrier dysfunction and inflammation in mice by modulating the gut microbiota. Mol Nutr Food Res 2021;65:e2000745.
[79] Lopez-Siles M, Duncan SH, Garcia-Gil LJ, Martinez-Medina M. *Faecalibacterium prausnitzii*: From microbiology to diagnostics and prognostics. ISME J 2017;11:841–52. doi: https://doi.org/10.1038/ismej.2016.176.
[80] Scorletti E, Afolabi PR, Miles EA, Smith DE, Almehmadi A, Alshathry A, et al. Synbiotics alter fecal microbiomes, but not liver fat or fibrosis, in a randomized trial of patients with nonalcoholic fatty liver disease. Gastroenterology 2020;158:1597–1610.e7. doi: https://doi.org/10.1053/j.gastro.2020.01.031.
[81] Tang RQ, Wei YR, Li YM, Chen WH, Chen HY, Wang QX, et al. Gut microbial profile is altered in primary biliary cholangitis and partially restored after UDCA therapy. Gut 2018;67:534–41. doi: https://doi.org/10.1136/gutjnl-2016-313332.